Melting curves of molecular hydrogen and molecular deuterium under high pressures between 20 and 373 K

V. Diatschenko* and C. W. Chu
Department of Physics and Energy Laboratory, University of Houston—University Park, Houston, Texas 77004

D. H. Liebenberg
National Science Foundation, Washington, D.C. 20550

D. A. Young and M. Ross
Lawrence Livermore National Laboratory, University of California, Livermore, California 94550

R. L. Mills
Los Alamos National Laboratory, University of California, Los Alamos, New Mexico 87545
(Received 22 October 1984; revised manuscript received 1 February 1985)

We determined the melting curve of molecular hydrogen and molecular deuterium at closely spaced intervals from 20 to 373 K by two different techniques using high-pressure diamond cells. The cells were loaded with liquid at low temperature or with compressed gas at room temperature. Empirical functions for the melting curves were evaluated from least-squares fits of the data. Values of the compressibility and Debye temperature were computed at melting, and the results are compared with those calculated from various theoretical models. The good agreement shows that the models are generally valid, although small systematic deviations may point the way toward refinements in modeling. Our study also demonstrates the need to determine a one-piece intermolecular potential valid over a wide pressure range by refitting all experimental data, including the shock data recently made available.

I. INTRODUCTION

In principle, it is possible to calculate the forces acting between molecules and thus predict the physical properties of molecular liquids and solids. In practice, however, this procedure is formidable, if not impossible, in view of the large number of molecules present. As an alternative to theoretical rigor, one can bypass *ab initio* calculations and search for an effective intermolecular potential which, with the aid of satisfactory statistical mechanical models, will explain the available experimental data and, perhaps, predict new experimental consequences.

High-pressure studies in molecular liquids and solids provide the most useful basis for deducing the effective intermolecular potential as a function of intermolecular spacing and for testing various theoretical models. Hydrogen, the simplest element in the Periodic Table, is especially attractive for this type of study. Consequently, the high-pressure properties of molecular hydrogen have been under intensive study for more than a decade. In particular, metallic hydrogen, which is of considerable scientific as well as potential technological significance, has been predicted to exist above a critical pressure.[1] Unfortunately, there is a large variance ranging from 0.25 to 20 Mbar among the calculated critical pressures for the metallization of hydrogen, as determined by the intersection pressure of the isotherms of Gibbs free energy versus pressure of the molecular and metallic phases of hydrogen.

Not until the recent advance of high-pressure diamond cells have high-pressure data on hydrogen and deuterium been extended[2] to above 25 kbar. In the past few years, a number of static high-pressure measurements on various thermodynamic properties of hydrogen and deuterium have been made[3,4] above 25 kbar and down to liquid-helium temperatures. Recently, shock-wave data,[5] more precise and accurate than previous data, have also become available. Several empirical effective intermolecular potentials for hydrogen have been proposed.[6–10] Despite differences in detail, they generally consist of an exponentially repulsive part and a modulated attractive multipole interaction (with a modulated triple-dipole term to account for the many-body effect in another case[9]). By employing statistical mechanical models, the free energies of hydrogen in both the solid and liquid phases are calculated.[9–11] The various thermodynamic properties are then determined by taking numerically the appropriate derivatives of the free-energy functions. Through the choice of proper adjustable parameters in the effective intermolecular potential, the theoretical models can, in general, reproduce reasonably well the experimental equation of state and Hugoniot curves for hydrogen and deuterium. However, the results also demonstrate that the effective potential obtained by fitting at small intermolecular spacings is always softer than that extrapolated from the potential at large intermolecular spacings.

Since the equation of state depends only on the derivatives of the free-energy function, the agreement between

the theory and experiment gives some credence to the effective intermolecular potentials and the theoretical models used. To predict a reliable critical pressure for the metallization of hydrogen requires information about the total values, not just the derivatives, of the free energies of both the molecular and metallic phases of hydrogen. Prior to the attainment of metallic hydrogen, the melting curve, which depends also on the total free energies, thus provides a sensitive check on the effective intermolecular potential and the theoretical models proposed for the prediction of metallization of hydrogen.

We have therefore, determined the melting curves of molecular hydrogen (H_2) and molecular deuterium (D_2) in small steps up to 78 kbar and 373 K, by employing high-pressure diamond cells[2] adapted for cryogenic operation.[4,12] No attempt was made to measure the para-ortho concentrations of the samples. As discussed later, such concentrations do not affect the results beyond our experimental uncertainty. To describe the melting lines of H_2 and D_2, a Simon equation and a modified form of this equation are proposed for interpolation as well as extrapolation. The Debye temperature Θ_D and compressibility κ along the melting curve are deduced. The results are compared with the various theoretical calculations.[6,8,10,11] Our comparison indicates that proposed intermolecular potentials are valid only over a limited pressure range in which they are calibrated and, therefore, extrapolation outside this pressure range can be done only with qualification. It should be noted that in view of the complexity of the intermolecular interactions and the relative simplicity of the model calculations, the general agreement between the experimental and calculated results is considered to be impressive, and suggests that there is general validity in the theoretical approach currently adopted for calculating the high-pressure properties of hydrogen and deuterium. However, small deviations in some of the calculations may call for refinements in the theoretical models, e.g., in the evaluation of the total Gibbs free energy G. It should also be pointed out that the melting of H_2 and D_2 has been investigated previously up to 164 K (Refs. 13–15) and at room temperature.[12,16,17] The present work represents the first successful attempt to determine melting in H_2 continuously up to 368 K and D_2 to 373 K. A portion of the preliminary data of this study has been reported briefly elsewhere.[4,18]

II. EXPERIMENTAL

Two different experimental techniques (A and B), employing a high-pressure Be-Cu diamond-anvil cell of the Mao-Bell[2] type, were developed for the present investigation down to cryogenic temperatures. Irrespective of the differences between the two techniques, the two sets of results obtained are in good agreement with each other. In technique A, we have used a Be-Cu cryogenic press for varying the pressure of the diamond-anvil cell at low temperature continuously by turning a pair of right- and left-handed screws outside the ^{4}He cryostate to eliminate the torque exerted on the press. Nonmagnetic, although weaker Be-Cu was used here for possible future application of the cell to magnetic measurements under pressure. *In situ* optical measurements, including direct visual observation, were accomplished by mounting on top of the diamond-anvil cell the objective of a specially designed telemicroscope with a magnification of ~ 120. The telemicroscope served as a conduit for both the "in" and "out" optical signals. A low-pass orange filter was inserted in the optical path for direct visual observation when the ruby chip was being excited optically by a He-Cd laser for pressure determinations. The sample chamber was a hole (200 μm in diameter) in a type-301 stainless-steel gasket, 250 μm thick, confined between two diamond anvils housed inside the high-pressure cell. Samples of H_2 or D_2 were loaded into the sample chambers by condensing the gases of purity 99.999% (H_2) and 99.5% (D_2) at ~ 16 and 19 K, respectively, and flooding the inside space of the high-pressure cell where the sample chamber was situated. The samples were then sealed by raising the bottom diamond anvil against the top one. Technique B involved a special design of a pressure vessel for loading and sealing the sample chamber in a diamond-anvil cell with different gases at a pressure of several kilobars at room temperature. The initial densities of the gases loaded exceeded those of the normal liquids. The diamond-anvil cell loaded with a gas sample was then removed from the pressure vessel and mounted in a lever mechanism in a cryostat for further compression and study at low temperatures. Details of this technique have been published elsewhere.[12]

To determine the pressure, we used the high-pressure ruby scale.[19] A laser-quality ruby chip of 15–20 μm in size was placed inside the sample chamber and excited by a He-Cd laser. The wavelength λ of the R_1-fluorescence line was then measured with a Jarrel-Ash monochromator and an RCA C-31034 photomultiplier. To enhance sensitivity and to simplify the procedure, the intensity of the R_1-fluorescence line was monitored continuously as a function of λ using a PAR lock-in amplifier with the exciting He-Cd laser beam chopped at a frequency of 27.5 Hz. This gave a ± 0.01 nm resolution in the λ measurements of the R_1-fluorescence line. In the present investigation, melting was determined at different temperatures and pressures. Since changes in temperature also affect the λ of the R_1 line, we determined the temperature-induced shift of λ, $\Delta\lambda(T) \equiv \lambda(4.2) - \lambda(T)$, between 4.2 and 380 K at 1 bar. The value of $\Delta\lambda(T)$ was found to remain 0 up to 77 K and to be well described above 77 K by the following expression:

$$1/\Delta\lambda(T) = \alpha (T/T_D)^4 \int_0^{T_D/D} [x^3/(e^x - 1)]dx \ , \qquad (1)$$

based on a two-phonon Raman-process model[20] with the electron-phonon parameter $\alpha = -4.08$ cm^{-1} and the Debye temperature of the ruby $T_D = 725$ K. The $\sim 1\%$ difference in α and $\sim 2.3\%$ difference in T_D between present values and those reported previously[20] may be attributed to the difference in ruby crystals. For instance, the respective Cr concentration of the ruby used in the present and previous studies was $\sim 0.55\%$ and $\sim 0.05\%$ by weight. The pressure-induced shift in λ, $\Delta\lambda(P) \equiv \lambda(P) - \lambda(0)$, at room temperature has been shown[21] to follow the relationship

$$P = 3.808\{[1 + \Delta\lambda(P)/\lambda(0)]^5 - 1\} \ , \qquad (2)$$

up to ~ 1.7 Mbar with P in kbar. To a good approximation, $\Delta\lambda(P)$ varies almost linearly with pressure at 0.036 nm/kbar for $P < 100$ kbar, according to Eq. (2). Up to 12 kbar, this pressure coefficient has been demonstrated[22] to be temperature independent between 4.2 and 358 K. Therefore, the sample pressure in the present investigation was determined by using the temperature-independent pressure coefficient of λ, 0.036 nm/kbar, and the pressure-induced shift $\Delta\lambda(P)=\Delta\lambda(P,T)-\Delta\lambda(T)$, where $\Delta\lambda(P,T)$ was the measured λ shift of the R_1 line at pressure P and temperature T from that at 1 bar and 4.2 K.

The sample temperature was controlled by a manganin heater wrapped around the exterior wall of the high-pressure cell. The heater was divided into three sections which permitted partial as well as entire cell heating. The temperature of the sample was determined with a chromel-alumel thermocouple attached to one of the diamond anvils through a pressure contact and located near the sample chamber. Since diamond is a superb thermal conductor, the temperature so obtained should represent well the temperature of the sample.

Usually, during a liquid-solid phase transition, crystals can be seen to grow, a pressure shift inside the sample chamber takes place as a result of the volume difference between the two phases, and enhanced diffused light scattering occurs because of the presence of a mixed-phase region when the temperature excursion rate in traversing the transition is high. One can thus determine the melting points of solidified gases as the temperature varies by at least three methods: (1) by visually observing the sudden appearance of crystals separated by liquid boundaries, (2) by measuring the pressure inside the sample chamber, and (3) by continuously monitoring the intensity of the R_1 line maximized at a fixed λ away from the transition. Since methods (2) and (3) are based on the volume difference between the liquid and solid phases, the phase transition manifests itself as a sharp rise (drop) in pressure on warming (cooling), as shown in Fig. 1 and an always drastic drop in the intensity of the R_1 line. Although all three methods were used in determining the melting points (T_m,P_m), method (1) was used only on cooling when a high rate of temperature change ($> \sim 10$ K/min) was achievable, and method (3) only below ~ 120 K when $\Delta\lambda(T)$ was small. All data points were determined by more than one method, with method (2) being the primary method of detection. The uncertainty in T_m obtained by method (1) was relatively large, depending on the cooling rate, but that by other methods was small (± 0.5 K). The observed temperature hysteresis of melting, on warming and cooling, was less than 3 K. The midpoint of the transition was taken as a point in the melting curve (T_m,P_m), as shown in Fig. 1. It should be noted that an intense He-Cd laser beam can cause significant local heating of the sample near the ruby manometer and thus a considerable error in determining the actual T_m. As a result, a detuned laser beam was used by us for pressure determination. The overall uncertainty was estimated to be ± 0.5 K in T_m and ± 0.6 kbar in P_m.

Although we easily obtained pressures of several hundred kilobars in our apparatus at low temperatures, difficulties were encountered at high temperatures. Repetitive thermal cycling often led to a failure of the diamond anvils under high pressure due to a slight misalignment caused by the difference between thermal expansion of the W-C rockers on which the diamond anvils were mounted, and that of the Be-Cu high-pressure pistons in which the W-C rockers were embedded. Thermal cycling was also found to have detrimental effects at high temperature on the type-301 stainless-steel gasket which served as the high-pressure sample chamber, presumably due to hydrogen embrittlement. The specific manganin heater used also imposed an upper limit on the temperature of the present study. With minor modifications, the experimental range of our techniques can be extended for measurements with continuous temperature and pressure variations.

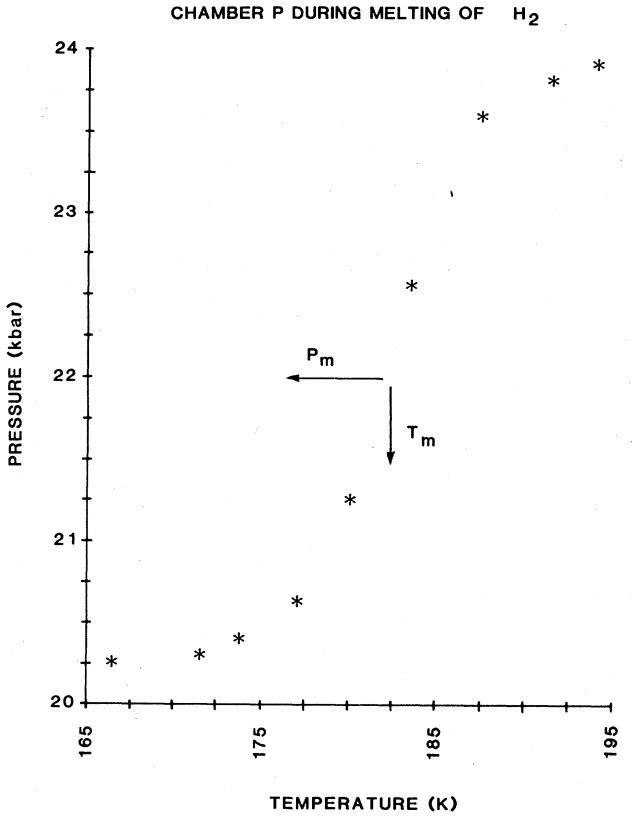

FIG. 1. Temperature dependence of the pressure inside the sample chamber during melting.

III. RESULTS

Using technique A, we determined 24 melting points of H_2 to 368 K and 77 kbar, and 14 melting points of D_2 to 302 K and 54 kbar. With technique B, we measured 9 melting points of D_2 to 373 K and 78 kbar. These melting points were obtained over a long period of time and on different samples. For instance, one sample of hydrogen was loaded and investigated for more than six months at 15 different pressures in an arbitrary pressuring sequence. For both isotopes, however, the scatter in the data points is small, especially for measurements using the same tech-

nique. The excellent self-consistency of the experimental results shows that the data are reversible for both pressure and temperature cyclings, and also demonstrates that any possible conversion between the paraspecies and orthospecies of H_2 and D_2 has a negligibly small effect on the experimental melting curves.

Our melting points of H_2 and D_2 are listed in Tables I and II, together with previous pre-diamond-anvil-cell low-pressure results[13–15] and those near room temperature determined in other laboratories.[12,16,17] Results of the present investigation are also shown in Figs. 2 and 3. Except for two room-temperature points in the melting curves of H_2 (Ref. 16) and D_2 (Ref. 17), results from different groups agree very well.

For the purpose of interpolation and extrapolation, Simon equations of the form $P_m = A + BT_m^c$ with P_m in kbar and T_m in K were proposed[15] to fit the experimental melting data up to 19 kbar with $A = -0.2442$, $B = 2.858 \times 10^{-3}$, and $c = 1.724$ for H_2; and $A = -0.5431$, $B = 3.66 \times 10^{-3}$, and $c = 1.677$ for D_2. These same equations describe well the present results with good accuracy up to ~ 50 kbar for H_2 and ~ 40 kbar for D_2. However, above 50 kbar, both the H_2 and D_2 data show an average 2.5% deviation from the above Simon equations, while the experimental uncertainties remain at $\sim 1.3\%$. By choosing new constants, we find that the $-H_2$ melting data (except for one point[16]) have a least-squares fit to the following modified Simon equation:[23]

$$P_m = -0.5149 + 1.702 \times 10^{-3}(T_m + 9.689)^{1.8077} \quad (3)$$

with a standard deviation of 0.20 kbar, displayed as a solid curve in Fig. 2. On the other hand, the D_2 data (except for one point[17]) can be least-squares fitted to the following Simon equation:

TABLE I. Pressure effects on T_m, Θ_D, and κ for H_2 along the melting curve. All are present work (determined by technique *A*) except where noted.

P_m (kbar)	T_m (K)	Θ_D (K)	$\kappa \times 10^{+2}$ (kbar^{-1})	P_m (kbar)	T_m (K)	Θ_D (K)	$\kappa \times 10^{+2}$ (kbar^{-1})
0.4	25[a]	151.1 (122.9[a])	18.2 (29.1[a])	16.20	151.5	451.8	1.56
0.48	26.6	156.6	16.7	16.44	152.6[b]	453.9 (394.2[b])	1.54 (1.56[b])
0.49	25.5[b]	152.8 (135[b])	17.7 (24.9[b])	16.77	154.0[e]	456.6 (440[e])	1.52
1.03	35.3[c]	184.9	11.4	18.71	163.9[e]	475.5 (457[e])	1.40 (1.46[e])
1.5	42[d]	204.4	8.99	22.2	183.5	512.1	1.21
1.63	43.8[c]	210.1	8.49	22.8	186.4	517.4	1.19
1.8	50[a]	227.3 (178.2[a])	7.07 (7.85[a])	22.93	182.0[b]	509.2 (444.9[b])	1.23 (1.13[b])
2.09	49.5[c]	226.0	7.17	24.3	191.0	525.8	1.15
2.99	58.9[c]	250.9	5.64	26.3	140[d]	429.4	1.73
4.02	67.4[c]	272.2	4.68	26.9	200[a]	542.2 (503.9[a])	1.09 (0.85[a])
4.73	75.04[e]	290.6 (280[e])	4.04 (3.76[e])	30.6	217.0	572.7	0.98
4.76	75.4[c]	291.5	4.02	31.8	223.4	584.0	0.95
4.8	70[d]	278.6	4.44	34.3	232.5	600.1	0.90
5.00	77.4[f]	296.2	3.87	35.3	237.6	609.0	0.88
5.20	77.4[f]	296.2	3.87	36.0	239.0	611.5	0.87
6.20	84.0[f]	311.5	3.46	39.8	250[a]	630.6 (586.8[a])	0.82 (0.63[a])
6.38	88.8[e]	322.4 (311[e])	3.20 (3.22[e])	40.0	253.7	637.0	0.81
6.90	90.6[f]	326.4	3.12	41.7	258.2	644.8	0.79
7.4	100[a]	347.1 (300.3[a])	2.72 (2.39[a])	44.3	269.0	663.4	0.75
7.76	100.8[e]	348.8 (336[e])	2.69 (2.92[e])	44.4	270.0	665.1	0.75
8.00	99.0[f]	344.9	2.76	51.6	294.1	706.3	0.68
8.09	102.3[b]	352.0 (307.0[b])	2.64 (2.98[b])	54.2	298[a]	712.9 (663.2[a])	0.67 (0.50[a])
8.20	102.5	352.5	2.63	55.0	298[g]	712.9	0.67
9.78	115.5[e]	379.9 (391[e])	2.24 (2.43[e])	56.4	309.0	731.5	0.64
9.80	112.0[f]	372.6	2.33	57.0	298.0[h]	712.9	0.67
10.05	113.0	374.7	2.31	59.6	300[i]	716.3 (695.5[i])	0.66 (0.47[i])
10.20	117.0[b]	383.0 (332.7[b])	2.20 (2.42[b])	62.0	325.0	758.5	0.61
11.77	125.8[e]	401.0 (388[e])	1.99	67.0	341.0	785.4	0.57
12.53	133.6[e]	416.7 (400[e])	1.84 (1.82[e])	69.5	347.0	795.4	0.56
13.33	137.8	425.1	1.77	77.1	368.0	830.6	0.53
13.41	135.4[b]	420.2 (366.7[b])	1.81 (1.88[b])	108.6	400[i]	884.0 (890.5[i])	0.49 (0.31[i])
14.63	143.8[e]	436.9 (420[e])	1.67 (1.75[e])	159.8	500[i]	1052 (996.1[i])	0.39 (0.24[i])
15.9	150[a]	448.9 (403.1[a])	1.58 (1.28[a])	169	280[d]	682.3	0.72

[a]Reference 11.
[b]Reference 27
[c]Reference 13.
[d]Reference 8.
[e]Reference 15.
[f]Reference 14.
[g]Reference 17.
[h]Reference 16.
[i]Reference 10

TABLE II. Pressure effects on T_m, Θ_D, and κ for D_2 along the melting curve. All are present work (determined by technique *A*, or where noted for technique *B*), except where otherwise indicated.

P_m (kbar)	T_m (K)	Θ_D (K)	$\kappa\times10^{+2}$ (kbar^{-1})
0.2	25[a]	109.0 (91.2[a])	17.3 (50.3[a])
0.57	30.0[b]	121.1	13.3
1.25	40.0[b]	143.3	8.79
2.0	25.0[a]	163.4 (144.1[a])	6.40 (6.50[a])
2.08	50.0[b]	163.4	6.40
3.04	60.0[b]	182.1	4.95
4.68	75.0[c]	208.3 (194[c])	3.63 (5.05[c])
4.70	75.19[c]	208.6 (194[c])	3.62 (3.93[c])
5.647	85.0[c]	224.7 (209[c])	3.06 (4.09[c])
7.010	94.7[c]	240.0 (224[c])	2.64 (3.40[c])
7.044	95.1[c]	240.6 (225[c])	2.63 (3.44[c])
7.963	102.1[c]	251.3 (236[c])	2.39 (3.41[c])
8.6	100[a]	248.1 (235.7[a])	2.45 (1.88[c])
10.021	115.5[c]	271.2 (254[c])	2.02 (2.78[c])
12.110	128.4[c]	289.6 (272[c])	1.76 (2.98[c])
12.80	131.5	294.0	1.71
12.99	134.2	297.9 (250.2[d])	1.66 (1.96[d])
13.47	136.3[c]	300.7 (283[c])	1.63 (2.31[c])
14.77	145.2[c]	312.9 (294[c])	1.50 (1.71[c])
15.00	143.5	310.6	1.52
15.38	147.8[d]	316.5 (265.1[d])	1.46 (1.69[d])
16.97	155.7[c]	327.0	1.37
17.00	156.0	327.4	1.37
17.47	159[d]	331.5 (277.2[d])	1.33 (1.51[d])
17.8	150[a]	319.4 (309.0[a])	1.44 (1.03[a])
22.2	180.4	359.3	1.14
22.65	185[d]	365.3 (303.9[d])	1.10 (1.2[d])
23.0	192.0[e]	374.0	1.05
26.2	199.0	382.8	1.00
28.5	210.5	397.1	0.94
31.9	224.8	414.6	0.86
33.6	232.5	423.9	0.83
34.7	236.0	428.1	0.82
35.8	244.0[e]	437.7	0.78
36.5	243.0	436.5	0.79
37.2	246.0[e]	440.1	0.78
41.1	260.2	456.9	0.73
43.1	250[a]	444.8 (438.6[a])	0.76 (0.51[a])
46.6	282[e]	482.3	0.66
48.4	285.8	486.7	0.65
50.1	290.8	492.5	0.64
50.5	298.0[e]	500.7	0.62
51.6	300.0[e]	503.3	0.62
53.4	302	505.3	0.61
57.2	295[a]	497.6 (487.5[a])	0.63 (0.41[a])
61.1	333.0[e]	540.9	0.55
78.0	372.5[e]	585.1	0.48

[a]Reference 11.
[b]Reference 13.
[c]Reference 15.
[d]Reference 27.
[e]Present work (technique *B*).

$$P_m=-0.5187+3.436\times10^{-3}T_m^{1.691} \quad (4)$$

with a standard deviation of 0.16 kbar, shown as a solid curve in Fig. 3.

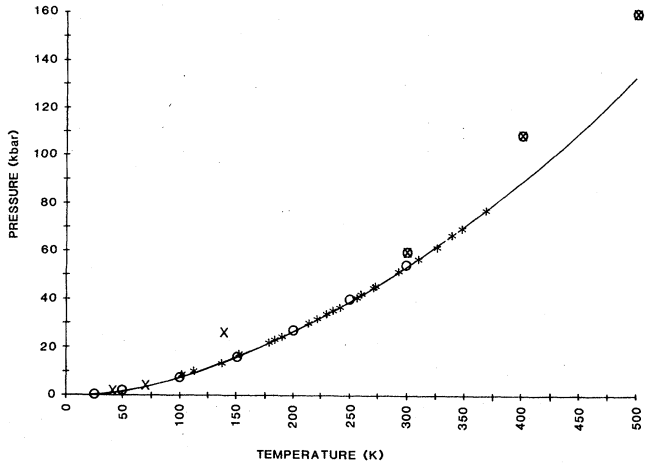

FIG. 2. Melting curve for H_2: * (technique *A*), present study; ○, Ref. 11; ⊗, Ref. 10; ×, Ref. 8; and ——, Eq. (3).

The Debye temperature Θ_D and the compressibility κ of solid H_2 and D_2 along the melting line are two interesting physical parameters that depend on the intermolecular potentials. We have, therefore, deduced both Θ_D and κ from the present melting data for comparison with proposed models. According to Lindemann's empirical relation, Θ_D and T_m are related by the expression

$$C^2=\Theta_D^2 V_S^{2/3} M/T_m \ , \quad (5)$$

where C is a constant, V_S the solid molar volume, and M the molecular weight. For deducing Θ_D from T_m, we have assumed the classical empirical value[24] of $C=116$ cm $K^{1/2}$ $g^{1/2}$ $mole^{5/6}$. This compares to a value of 114 for low-pressure hydrogen[25] and 117 for helium.[26] Recent model calculations[10,11] show that above ~100 K for H_2 and D_2, C approaches the classical value of 116 from below. This has been attributed to the quantum effect, which decreases with increasing temperature. Since the

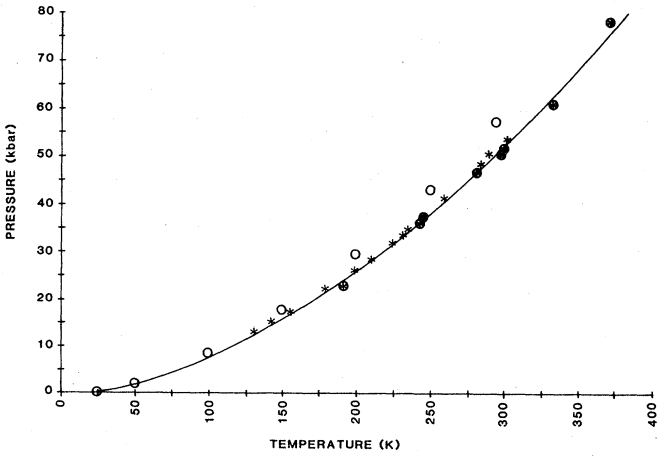

FIG. 3. Melting curve for D_2: * (technique *A*) and ⊗ (technique *B*), present study; ○, Ref. 11; and ——, Eq. (4).

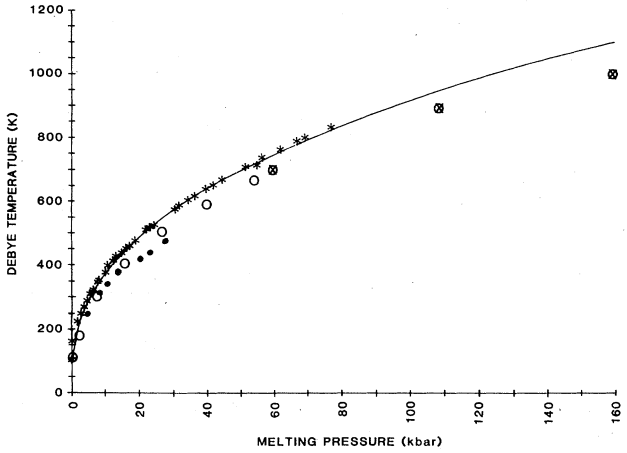

FIG. 4. Θ_D for H_2: *, present study; ○, Ref. 11; ⊗, Ref. 10; ——, Eq. (8); and ●, Ref. 27.

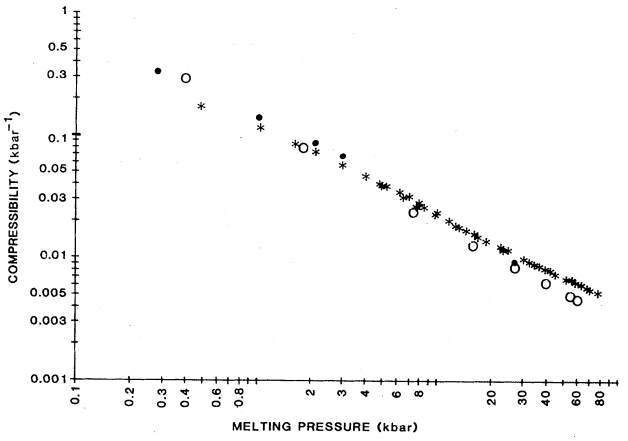

FIG. 6. κ for H_2: *, present study; ○, Ref. 11; ●, Ref. 27.

primary interest of the present investigation is in temperatures above 100 K, the use of $C=116$ is justified. To obtain the necessary values of V_S along the melting line, a least-squares analysis has been performed on the previous solid-volume data below 20 kbar (Ref. 15) and at ~50 kbar (Ref. 17), resulting in the following empirical equations:

$$V_S=35.8296-4.9134\ln T_m \quad \text{for } H_2 \tag{6}$$

and

$$V_S=32.9693-4.3863\ln T_m \quad \text{for } D_2\ , \tag{7}$$

with a standard deviation of 0.067 cm^3/mole for Eq. (6) and 0.064 cm^3/mole for Eq. (7). Values of Θ_D so deduced are given in Tables I and II and displayed in Figs. 4 and 5. As shown in these same figures, they can be represented by

$$\Theta_D=85.389-0.729P_m+98.832P_m^{0.481} \quad \text{for } H_2 \tag{8}$$

and

$$\Theta_D=74.650+65.298P_m^{0.476} \quad \text{for } D_2\ . \tag{9}$$

This represents an extension of the previous Θ_D results similarly obtained[15] below 20 kbar. The value of κ along the melting line of H_2 and D_2 can be calculated from

$$\kappa=-(1/V_S)(\partial V_S/\partial P_m)$$
$$=(1/V_S)(\partial V_S/\partial T_m)/(\partial P_m/T_m) \tag{10}$$

with V_S given by Eqs. (6) and (7), and P_m by Eqs. (3) and (4). The deduced values of κ are given in Tables I and II and shown in Figs. 6 and 7. The difference between the κ's of H_2 and D_2 appears to be very small. Earlier results[15,17,27] are also included in Tables I and II for comparison.

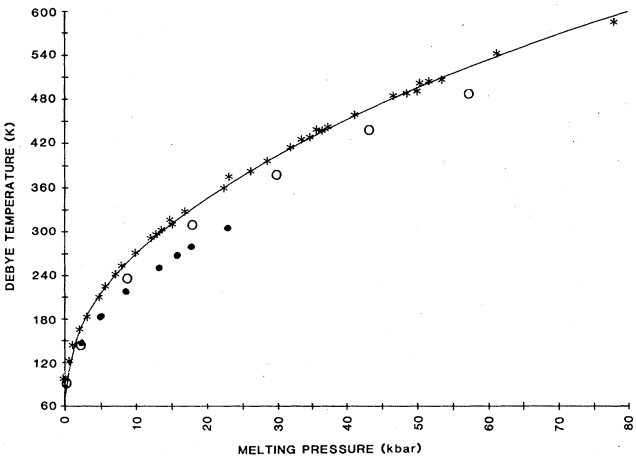

FIG. 5. Θ_D for D_2: *, present study; ○, Ref. 11; ——, Eq. (9); and ●, Ref. 27.

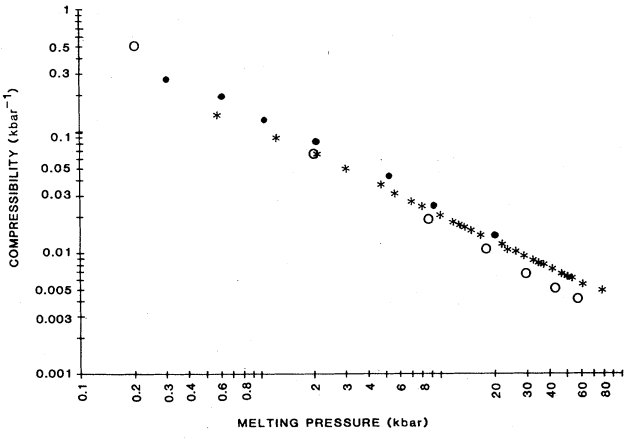

FIG. 7. κ for D_2: *, present study; ○, Ref. 11; ●, Ref. 27.

IV. DISCUSSION

The previous reported melting curves for H_2 and D_2 below 5 kbar were carefully measured[13] and fitted[27,28] to various experimental functions. However, to give uniform representation over our large pressure range, we have included only a few of these low-pressure melting points, in Tables I and II. As is evident from Tables I and II, the agreement among various sets of data, when overlap in temperature and pressure exists, is good. In particular, the excellent agreement of the previous data[15] below 20 kbar, where absolute pressure was determined, with the present data, where the pressure was determined on a ruby scale, demonstrates that the ruby pressure scale can be used as a secondary absolute pressure scale even at low temperatures, provided the temperature effect described in Sec. II is properly taken into consideration. The Simon equation (3) and the modified Simon equation (4), proposed by us, result from least-squares fits from the experimental data in Tables I and II and thus represent the empirical functions that best describe the existing melting points of H_2 and D_2 to date.

Several attempts have been made to predict the melting temperatures at high pressures. However, exact calculations are restricted to computer simulations for many-body (although smaller number than real) systems with simple interparticle potentials. Only in the past few years has it been possible to predict P_m and T_m from model calculations (rather than from the phenomenological Lindemann law and Simon equation). All such model calculations use effective intermolecular potentials which are derived by fitting the equation of state and some thermodynamic properties. In 1974, an effective intermolecular potential was found to reproduce well the Hugoniot of H_2 from shock experiments.[6] It had also been shown[29] that the packing fraction $\eta=\pi d^3\rho/6$, with d being the hard-sphere diameter and ρ the particle density, should have the constant value 0.468 along the melting line. From the above-mentioned intermolecular potential, several melting points of H_2 were then obtained[6] by finding the pressures in the liquid phase at a number of temperatures for which $\eta=0.468$, in the framework of the modified Mansoori-Canfield variational perturbation theory.[30] The pressures so calculated are higher than those shown in Table I and Fig. 2, by about 38 kbar at 250 K for H_2. Still larger discrepancies ($\sim$170 kbar calculated versus 52 kbar experimental) were obtained[8] near room temperature, on the basis of the equations of state for the solid and liquid phases of molecular hydrogen, which were fitted with shock data to another type of interparticle potential. Recent advances, however, in statistical theory coupled with more accurate intermolecular potentials could make possible the accurate calculations of the melting curves of molecular solids from first principles, namely, by locating the intersection pressure of the isotherms of G of the solid and liquid phases.[31]

To reproduce the low-temperature solid isotherms of H_2 and D_2 at high pressures, several intermolecular potentials consisting basically of exponential short-range repulsion and multipole attraction with proper modulation at various distances have been proposed. For instance, taking the spherical average of the self-consistent field and configuration interaction calculations, Etters and coworkers[32] provided a potential exponentially repulsive at short range with a multipole attraction of the form $-(C_6/r^6+C_8/r^8)$, which is modulated by $f(r)$, being 1 at large r and diminishing to 0 at small r. The 4.2-K solid isotherm of H_2 at high pressures was successfully reproduced[33] by adjusting the different parameters in the potential, e.g., C_6 and C_8. Later, Rayleigh-Schrödinger perturbation calculations[34] gave multipole constants, e.g., C_8 and C_{10}, that are different from those empirically determined.[32] In addition, the C_{10}/r^{10} potential was shown to be too large to be neglected. By adopting these new multipole constants ($C_6=12.14$, $C_8=215.2$, and $C_{10}=4813.9$, all in atomic units) and including the leading term of the triple-dipole interaction to account for many-body effects, Silvera and Goldman[9] proposed the following potential for H_2 and D_2:

$$\phi_{\mathrm{SG}}(r)=\exp(\alpha-\beta r-\gamma r^2) -(C_6/r^6+C_8/r^8+C_{10}/r^{10})f(r)+(C_9/r^9)f(r)\ , \tag{11}$$

where

$$f(r)=\begin{cases}\exp[(1.28r_m/r)-1]^2 & \text{for } r<1.28r_m,\\ 1 & \text{for } r>1.28r_m,\end{cases}$$

and r_m is the position of the well minimum of Eq. (11), excluding the last and many-body term. The value of $C_9=143.1$ a.u. was determined by comparing the triple-dipole interaction and the polarizability of H_2 with the rare gases. By fitting the low-temperature high-pressure solid D_2 data[33] to Eq. (9), the adjustable parameters were found to be $\alpha=1.713$, $\beta=1.5671$, and $\gamma=0.009\,93$, all in atomic units. It should be noted that the $1/r^9$ potential is positive and has been inferred by the observed volume dependence of the sound velocity in solid H_2 and D_2.[35]

Young and Ross[11] recently used the semiempirical Silvera-Goldman[9] potential, ϕ_{SG}, and computed G for both the solid and liquid phases of H_2 and D_2 under pressure up to 300 K. The calculations were made from quasiharmonic lattice dynamics corrected by anharmonic terms for the solid and a modified hard-sphere variational perturbation theory with a quantum correction for the liquid. The melting points were then determined by plotting isotherms of G versus P for the solid and liquid phases and locating the points of intersection. The results are given in Tables I and II, and displayed in Figs. 2 and 3. It is evident that the calculated results, when compared to the present measurements, show a very good agreement throughout the experimental range for H_2, but good agreement only below $\sim$150 K for D_2. Above 150 K the D_2 calculations show a rapidly increasing disagreement, and at 300 K are in disagreement by $\sim$11%. In view of the high accuracy required in computing G for the two phases for determining the melting curve, the success of the models of solid and liquid phases used, perhaps, should not be underestimated by the deviation mentioned above. An attempt[36] has been made to deduce from the existing experimental data[14,34,35] the G's of the H_2 and D_2 solids at 4 K and liquids at 200 and 298 K under pressures, by choosing 0 K for solids and the triple points for

liquids as the reference points of G. For solid H_2 and D_2 at 4 K, the deduced G's as a function of pressure are slightly above, but almost parallel to, the ones calculated by Young.[37] For the liquids, there is agreement between the deduced and calculated values for H_2 but not for D_2. For liquid D_2, the deduced values are $\sim 10\%$ larger than the calculated ones. By assuming that such a relative behavior of the calculated G's with respect to the deduced ones persists throughout our experimental range, the disagreement between the experimental and calculated melting curve of D_2 shown in Fig. 3 can be qualitatively understood.

Comparison of the experimental H_2 and D_2 melting curves shows that the H_2 curve always has a higher pressure for any given temperature. Although the theory correctly predicts the bulk of the isotope effect in the liquid and solid equations of state,[11] it incorrectly predicts the isotope effect in melting and reverses the relationship between the H_2 and D_2 melting curves. This accounts for the difference in the accuracy of the theoretical H_2 and D_2 melting curves. This error is a subtle effect which must arise from the quantum terms in the solid and liquid free-energy models. Further research will be required to resolve this problem.

Following the recent attainment[5] of accurate shock results on H_2 and D_2, Ross *et al.*[10] found that ϕ_{SG} is too stiff to describe the Hugoniot and that two different forms of intermolecular potential are needed to explain the experimental data. They extended their model calculation[11] of the H_2 melting curve to 480 kbar using the following Young-Ross[10] potential:

$$\phi_{YR}(r)=\begin{cases}\phi_{SG}(r) & \text{for } r>r_c,\\ A\exp[-B(r-r_c)-C(r-r_c)^2-D(r-r_c)^3-E(r-r_c)^3(r-r_1)] & \text{for } r<r_c\end{cases} \tag{12}$$

with $A=3.988\,23\times10^{-1}$ erg, $B=4.769\,40$ Å^{-1}, $C=2.254\,57$ Å^{-2}, $D=0.955\,189$ Å^{-3}, $E=0.248\,158$ Å^{-4}, $r_1=1.2$ Å, and $r_c=2.55$ Å. The ϕ_{YR} is softer than ϕ_{SG} at small r and becomes ϕ_{SG} at large r. The calculated melting points at up to 500 K are included in Table I and Fig. 2. The corresponding melting pressures are higher than the experimental values and the deviation increases with pressure, at least when compared with the extrapolated pressures above 77 kbar from Eq. (3). Since the models of solid and liquid used for the calculations are the same, the disagreement may have arisen from choosing $r_c=2.55$ Å that is too large. This makes the potential too soft in the region probed by static pressure experiments. For instance, a static experiment even at 20 kbar and 300 K can probe the potential for $r\sim2.4$ Å, which is smaller than the r_c chosen. The potential in Eq. (12) is a preliminary attempt to fit the available shock and static equation-of-state data. It is clear that a more carefully fitted, one-piece potential is needed to predict correctly the melting curve.

Ross and co-workers[10,11] have calculated Θ_D using the force constant derived from ϕ_{SG} below 54 kbar and from ϕ_{YR} above 59.6 kbar. By using the empirical volume dependence of the optical phonon, Driessen and Silvera[27] have also calculated Θ_D up to 27 kbar. The results have been shown in Tables I and II, as well as in Figs. 4 and 5. Since it has been found[10,11] that the Lindemann constant C is not a constant in our pressure range, the deviation of the calculated Θ_D from our Θ_D deduced from the classical constant is not surprising. It is known that the classical value of $C=116$ is valid only for a harmonic or Debye solid with negligibly small anharmonic and quantum effects. However, solid H_2 and D_2 have been shown to exhibit large anharmonic and quantum effects, especially at low pressures and temperatures. This is consistent with recent calculations[10,11] of C approaching the classical constant of 116 from below with increasing pressure and temperature. Our deduced values of Θ_D under pressure should therefore be treated only qualitatively. On the other hand, whether a full lattice-dynamics calculation of Θ_D will show a different behavior of C under pressure from that reported remains to be seen. For a Debye solid, there exists an isotope effect in which Θ_D scales as $M^{-1/2}$, M being the isotopic mass. The ratio R of the Θ_D for H_2 to that for D_2 might then be expected to be $\sqrt{2}=1.414$. We have calculated Θ_D for H_2 at pressures where the melting points of D_2 have been measured, using the least-squares-fitted equations (3) and (8). The value of R so determined is indeed 1.414 ± 0.004. The significance of this ratio, however, is tempered by the fact that Θ_D for H_2 and D_2 are calculated primarily on the basis of the Lindemann law, and there are only small differences between the T_m's and V_S's of H_2 and D_2 solids.

We have also least-squares fitted the calculated V_S-P_m results[11] and obtained the empirical relations

$$V_S=17.461-2.278\ln P_m \quad \text{for } H_2 \tag{13}$$

and

$$V_S=16.217-1.945\ln P_m \quad \text{for } D_2\,, \tag{14}$$

where V_S is in cm^3 and P_m in kbar. Values of κ calculated from Eqs. (13) and (14) are compared with the experimentally deduced values for both H_2 and D_2 in Figs. 6 and 7. Since κ represents a second-order effect in testing the interparticle potential and the model calculations, the general agreement is impressive. However, a slight deviation between the calculated[11] and deduced values exists at pressures away from 2 kbar as is evident in Fig. 6. This may result because Φ_{SG} was calibrated at 2 kbar. On the other hand, disagreement is also evident from the same figures between our deduced values and those obtained by Driessen and Silvera.[27] The reason is unknown.

ACKNOWLEDGMENT

The work performed at Houston was supported in part by the National Science Foundation (Low Temperature Physics Program) under Grant No. DMR-82-04173 and by the Energy Laboratory of the University of Houston, and the work at Los Alamos National Laboratory and Lawrence Livermore National Laboratory was performed under the auspices of the U.S. Department of Energy.

---

*Present address: Texaco Research Center, Houston, TX 77215-0070.

[1]For a review, see A. L. Ruoff, in *High Pressure and Low Temperature Physics,* edited by C. W. Chu and J. A. Woodlam (Plenum, New York, 1978), p. 1; A. K. McMahan, in *High Pressure and Low Temperature Physics,* p. 24; J. Oliva and N. W. Ashcroft, Phys. Rev. B **23**, 6399 (1981).

[2]H. K. Mao and P. M. Bell, Science **200**, 1145 (1978), and references therein.

[3]R. J. Wijngaarden and I. F. Silvera, Phys. Rev. Lett. **44**, 456 (1980); I. F. Silvera and R. J. Wijngaarden, *ibid.* **47**, 39 (1981); J. Van Straaten, R. J. Wijngaarden, and I. F. Silvera, *ibid.* **48**, 97 (1982).

[4]V. Diatschenko and C. W. Chu, Science **212**, 1393 (1981).

[5]W. J. Nellis, A. C. Mitchell, and M. Van Thiel, J. Chem. Phys. **79**, 1480 (1983).

[6]M. Ross, J. Chem. Phys. **60**, 3634 (1974).

[7]W. England, R. Etters, J. Raich, and R. Danilowitz, Phys. Rev. Lett. **32**, 758 (1974); R. D. Etters, R. Danilowitz, and W. England, Phys. Rev. A **12**, 2199 (1975).

[8]F. V. Grigorev, S. B. Kormer, O. L. Mikhailova, A. P. Tolochko, and V. D. Urlin, Zh. Eksp. Teor. Fiz. **69**, 743 (1975) [Sov. Phys.—JETP **42**, 378 (1975)].

[9]I. F. Silvera and V. V. Goldman, J. Chem. Phys. **69**, 4209 (1978).

[10]M. Ross, F. H. Ree, and D. A. Young, J. Chem. Phys. **79**, 1487 (1983), and references therein.

[11]D. Young and M. Ross, J. Chem. Phys. **74**, 6950 (1981).

[12]R. L. Mills, D. H. Liebenberg, J. C. Bronson, and L. C. Schmidt, Rev. Sci. Instrum. **51**, 891 (1980).

[13]F. Simon, M. Ruheman, and W. A. M. Edwards, Z. Phys. Chem. B **6**, 331 (1930); R. L. Mills and E. R. Grilly, Phys. Rev. **101**, 1246 (1956).

[14]V. V. Kechin, A. I. Likhter, Yu. M. Pavlyuchenko, L. Z. Ponizovskii, and A. N. Utyuzh, Zh. Eksp. Teor. Fiz. **72**, 345 (1977) [Sov. Phys.—JETP **45**, 182 (1977)].

[15]D. H. Liebenberg, R. L. Mills, and J. C. Bronson, Phys. Rev. B **18**, 2663 (1978).

[16]H. K. Mao and P. M. Bell, Science **203**, 1004 (1979).

[17]H. Shimizu, E. M. Brody, H. K. Mao, and P. M. Bell, Phys. Rev. Lett. **47**, 128 (1981); H. K. Mao, E. M. Brody, H. Shimizu, and P. M. Bell, Geophys. Lab. Ann. Report, 8-81, No. 1855, p. 286 (unpublished).

[18]V. Diatschenko and C. W. Chu, Bull. Am. Phys. Soc. **26**, 322 (1981); **27**, 324 (1982).

[19]R. A. Forman, G. J. Piermarini, J. D. Barnett, and S. Block, Science **176**, 284 (1972).

[20]D. E. McCumber and M. D. Sturge, J. Appl. Phys. **34**, 1682 (1963).

[21]H. K. Mao, P. M. Bell, J. W. Shaner, and D. J. Steinberg, J. Appl. Phys. **49**, 3476 (1978).

[22]R. A. Noack and W. B. Holzapfel, *High Pressure Science and Technology,* edited by K. D. Timmerhaus and M. S. Barber (Plenum, New York, 1979), Vol. 1, p. 748.

[23]R. K. Crawford and W. B. Daniels, J. Chem. Phys. **55**, 5651 (1971).

[24]R. L. Mills, D. H. Liebenberg, and J. C. Bronson, J. Chem. Phys. **63**, 1199 (1975).

[25]C. Domb, Nuovo Cimento Suppl. **9**, 9 (1958).

[26]J. S. Dugdale, *Physics of High Pressure and the Condensed Phase,* edited by A. Van Itterbeek (North-Holland, Amsterdam, 1965), p. 421.

[27]A. Driessen and I. Silvera, J. Low Temp. Phys. **54**, 361 (1984), and references therein.

[28]H. W. Woolley, R. B. Scott and F. G. Brickwedde, J. Res. Nat. Bur. Stand. **41**, 379 (1948); R. D. Goodwin, Cryogenics **2**, 353 (1962).

[29]N. W. Ashcroft and J. Lekner, Phys. Rev. **145**, 83 (1966).

[30]G. A. Mansoori and F. B. Canfield, J. Chem. Phys. **51**, 4958 (1969); M. Ross, *ibid.* **71**, 1567 (1979).

[31]M. Ross and D. A. Young, Phys. Lett. **78A**, 463 (1980).

[32]W. England, R. Etters, J. Raich, and R. Danilowitz, Phys. Rev. Lett. **32**, 758 (1974); R. Etters, R. Danilowitz, and E. England, Phys. Rev. A **12**, 2199 (1975).

[33]M. S. Anderson and C. A. Swenson, Phys. Rev. B **10**, 5184 (1984).

[34]W. Meyer, Chem. Phys. **17**, 27 (1976).

[35]D. H. Liebenberg, R. L. Mills and J. C. Bronson, Los Alamos Scientific Laboratory Report No. LA-6645-MS, 1977 (unpublished) and Report No. LA-7007-MS, 1978 (unpublished); and D. H. Liebenberg (private communication).

[36]V. Diatschenko, Ph.D. Dissertation, University of Houston, 1982 (unpublished).

[37]D. A. Young (unpublished).